Electronic Supplementary Material (ESI) for ChemComm.

Supplementary Information

Mechanistic insights into asymmetric transfer hydrogenation of pyruvic acid catalysed by chiral osmium complexes with formic acid assisted proton transfer

Wan Wang,[a,b] Xinzheng Yang* [a,b]

[a] Beijing National Laboratory for Molecular Sciences, State Key Laboratory for Structural Chemistry of Unstable and Stable Species, CAS Research/Education Center for Excellence in Molecular Sciences, Institute of Chemistry Chinese Academy of Sciences, Beijing 100190, P. R. China.

[b] University of Chinese Academy of Sciences, Beijing 100049, P. R. China

1. Theoretical methods

The Gaussian 09 suite of ab initio programs[1] was employed to perform DFT calculations using the hybrid meta-GGA level M06 functional[2] in conjugation with 6-31G(d) basis set[3, 4] for small atoms, and Stuttgart relativistic effective core potential basis set for Os (ECP60MDF).[5] The accuracy of numerical integrations is at the ultrafine grid (99,590) level. Geometric optimizations were performed without restriction in formic acid (ε = 51.1). The integral equation formalism polarizable continuum (IEFPCM) solvation model[6] with the SMD radii[7] were used for solvent effect corrections. Thermal corrections were obtained by frequency calculations on optimized structures within the harmonic potential approximation under 298.15 K and 1 atm pressure. The optimized structures were confirmed to have no imaginary vibrational mode for all equilibrium structures and only one imaginary vibrational mode for each transition state. Transition states were further characterized by intrinsic reaction coordinate (IRC) calculations to affirm that the correct stationary points were connected. The 3D molecular structures were drawn by using the JIMP2 molecular visualizing and manipulating program.[8]

Activation strain model (ASM), also known as the *distortion/interaction model*, is a computational method which gives an insight into the physical factors controlling the potential activation barriers among the competing pathways.[9, 10] This method is a fragment approach to predict the influences on activation barriers of chemical reactions.[11] Along the reaction coordinate ζ, the relative energy $\Delta E(\zeta)$ can be decomposed into the strain energy $\Delta E_{\text{strain}}(\zeta)$ and interaction $\Delta E_{\text{int}}(\zeta)$. The former derives from the deformed reactants during the transformation of equilibrium geometry to the transition state, and the latter comes from the electronic structure as well as the interaction between the increasingly deformed reactants:

$$\Delta E(\zeta) = \Delta E_{\text{strain}}(\zeta) + \Delta E_{\text{int}}(\zeta)$$

2. Evaluation of density functionals

Table S1. Absolute and relative free energies of **$TS_{2,3\text{-}R}$** and **$TS_{2,3\text{-}S}$** with different functionals.

Functionals	Absolute free energies (Hartree)		Relative energies (kcal mol^{-1})
	$TS_{2,3\text{-}R}$	**$TS_{2,3\text{-}S}$**	**$TS_{2,3\text{-}R} \rightarrow TS_{2,3\text{-}S}$**
TPSS	-2483.911319	-2483.910449	0.5
TPSS-D3	-2484.038631	-2484.037163	0.9
B3LYP	-2483.543424	-2483.541050	1.5
B3LYP-D3	-2483.691637	-2483.689928	1.1
B3PW91	-2482.807880	-2482.806182	1.1
B3PW91-D3	-2482.977159	-2482.974311	1.8
ωB97X	-2483.042475	-2483.042316	0.1
ωB97X-D	-2482.972605	-2482.971261	0.8
PBEh1PBE	-2481.333522	-2481.330876	1.7
M06	-2482.172058	-2482.169444	1.6

In order to evaluate the dependence of density functionals of this osmium system, especially the effect of dispersion on the weak interactions responsible for enantioselectivity, we calculated the relative free energies of between **$TS_{2,3\text{-}R}$** and **$TS_{2,3\text{-}S}$** (Table S1), as well as between the **5'** and **$TS_{5,1}$** (Table S2) using nine other widely-used and/or recently developed functionals, including TPSS,[12] B3LYP,[13,14] B3PW91,[15,16] and these functionals with Grimme's GD3 dispersion correction[17], TPSS-D3, B3LYP-D3, B3PW91-D3, as well as ωB97X,[18] ωB97X-D[19] and PBEh1PBE[20] functionals. All other computational details are the same as described in the above section.

As shown in Table S1, the relative energies differences between $\mathbf{TS_{2,3\text{-}R}}$ and $\mathbf{TS_{2,3\text{-}S}}$ obtained with or without Grimme's dispersion correction (including ωB97X and ωB97X-D) are less than 1.0 kcal mol^{-1}, and all functionals have similar enantioselectivity. Table S2 shows the difference of relative energies between **5'** and $\mathbf{TS_{5,1}}$ obtained with all functionals is less than 7.7 kcal mol^{-1}. The relative free energy differences caused by the dispersion correction are less than 2.5 kcal/mol. The M06 result of 16.6 kcal mol^{-1} is in the middle and very close to the results of B3LYP, B3LYP-D3, B3PW91, B3PW91-D3 and PBEh1PBE functionals. More importantly, the total free energy barrier calculated by using the M06 functional matches well with the observed reaction rate. Therefore, we believe M06 is a suitable functional for the computational study of this Os system.

Table S2. Absolute and relative free energies of **5'** and $\mathbf{TS_{5,1}}$ with different functionals.

Functionals	Absolute free energies (Hartree)		Relative free energies (kcal mol^{-1})
	5'	$\mathbf{TS_{5,1}}$	**5'** → $\mathbf{TS_{5,1}}$
TPSS	-2140.375823	-2140.353318	14.1
TPSS-D3	-2140.480140	-2140.457581	14.2
B3LYP	-2140.053348	-2140.027830	16.0
B3LYP-D3	-2140.175722	-2140.150020	16.1
B3PW91	-2139.449762	-2139.423999	16.2
B3PW91-D3	-2139.589021	-2139.562987	16.3
ωB97X	-2139.635726	-2139.600979	21.8
ωB97X-D	-2139.579978	-2139.549216	19.3
PBEh1PBE	-2138.183205	-2138.156137	17.0
M06	-2138.858290	-2138.831787	16.6

3. Evaluation of basis sets

Table S3. Absolute and relative electronic energies of $\mathbf{TS_{2,3\text{-}R}}$ and $\mathbf{TS_{2,3\text{-}S}}$ with different basis sets.

Basis sets	Absolute electronic energies (Hartree)		Δ*E* (kcal mol^{-1})
	$\mathbf{TS_{2,3\text{-}R}}$	$\mathbf{TS_{2,3\text{-}S}}$	
6-31G(d)\MDF	−2482.808777	−2482.805077	−2.3
6-31G(d,p)\MDF	−2482.873662	−2482.870584	−1.9
6-31+G(d,p)\MDF	−2482.961035	−2482.957858	−2.0
6-31++G(d,p)\MDF	−2482.963159	−2482.959808	−2.1
6-31G(d)\MWB	−2482.636850	−2482.633943	−1.8

In order to evaluate the accuracy of basis sets used in our DFT calculations, we used four larger basis sets to calculate the single point energies of key transition states in the enantio-determining steps, 6-31G(d,p) basis set for small atoms and ECP60MDF for Os, 6-31+G(d,p) basis set for small atoms and ECP60MDF for Os, 6-31++G(d,p) basis set for small atoms and ECP60MDF for Os, 6-31G(d) basis set for small atoms and ECP60MWB[21] for Os. As shown in Table S3, the electronic energy differences between $\mathbf{TS_{2,3\text{-}R}}$ and $\mathbf{TS_{2,3\text{-}S}}$ obtained by using different basis sets are from −1.8 to −2.3 kcal mol^{-1}. Such a 0.5 kcal mol^{-1} range of difference indicates that the 6-31G(d) and ECP60MDF basis sets used in this study are large enough for the DFT calculations of this Os system.

4. Isomers of catalyst 1

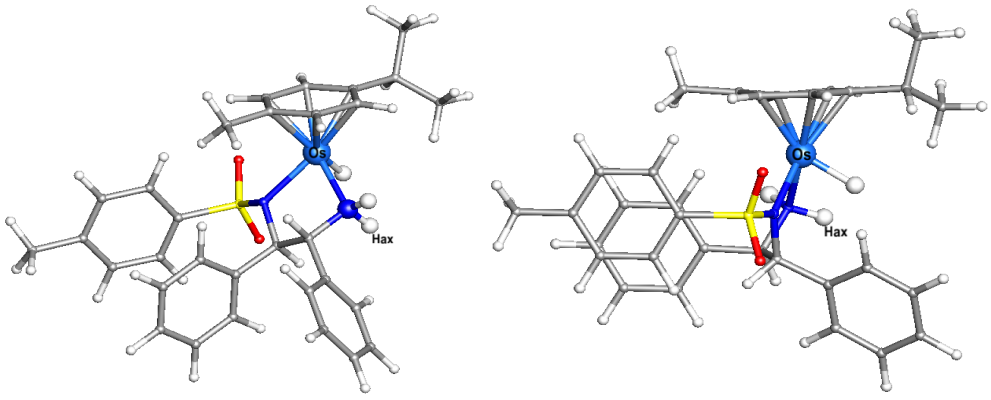

1 **1'**

Figure S1. Optimized structures of **1** and its isomer **1'**.

In order to find out the most stable structure of the chiral catalyst **1**, we examined its isomer **1'**, in which the two phenyl group in the five numbered Os–N–C–C–N ring are at the axial positions (Figure S1). The optimized structure of **1'** is 3.3 kcal mol^{-1} less stable than **1**, so we believe **1** is the real catalyst in the reaction.

5. The influence of solvent FA molecule.

In order to have a better understanding of the influence of solvent FA molecule in the reaction, we also considered the situations without the participation of FA and with the presence of two FA molecules for hydride and proton transfer in our computational study. The mechanism for the hydrogenation of PA catalysed by **1** without the participation of extra FA molecule for proton transfer is shown in Scheme S1. The corresponding free energy profile is shown in Figure S2. DFT

calculation results suggest that the hydrogen transfer proceeds via two steps, hydride transfer from metal to carbonyl carbon and proton transfer from the axial hydrogen in nitrogen ligand to the carbonyl oxygen. The EDSs are still the metal to the carbonyl carbon hydride transfer process, but the ion-pair intermediates **3'** have the highest relative free energies. This result further demonstrates the importance of solvent FA molecule in the asymmetric reduction of PA.

Scheme S1. Proposed mechanism for the hydrogenation of PA catalysed by **1** without the participation of formic acid.

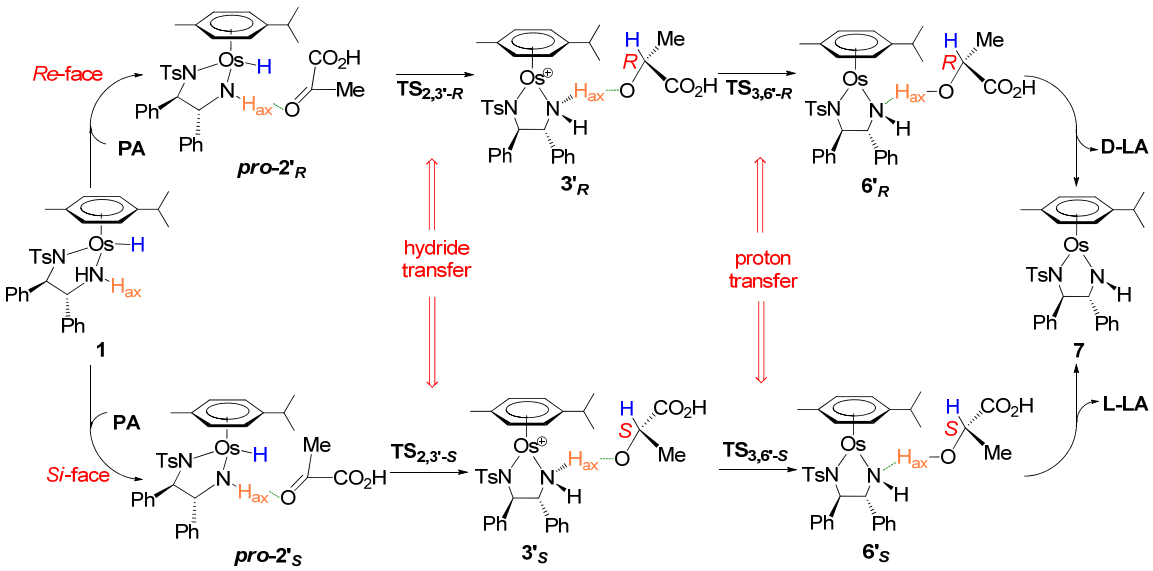

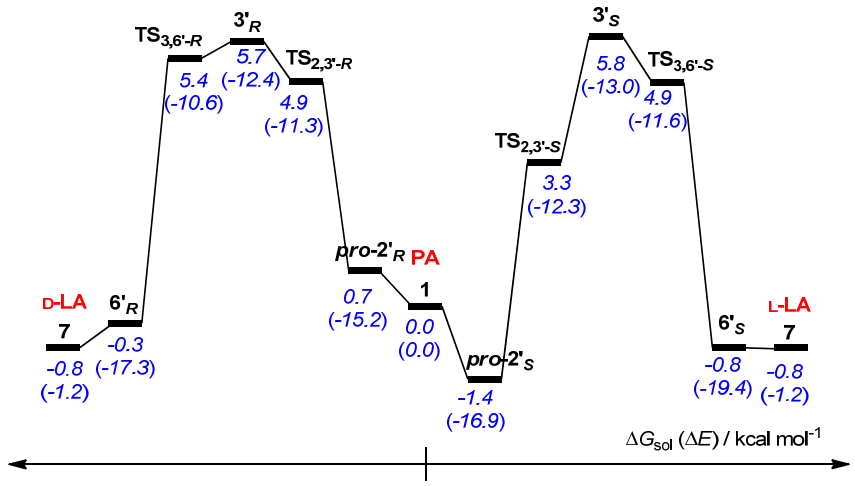

Figure S2. Energy profile for the hydrogenation of PA catalysed by **1** without the participation of formic acid. The relative electronic energies are shown in parentheses.

Scheme S2. Proposed mechanism for the hydrogenation of PA catalysed by **1** with the presence of two FA molecule.

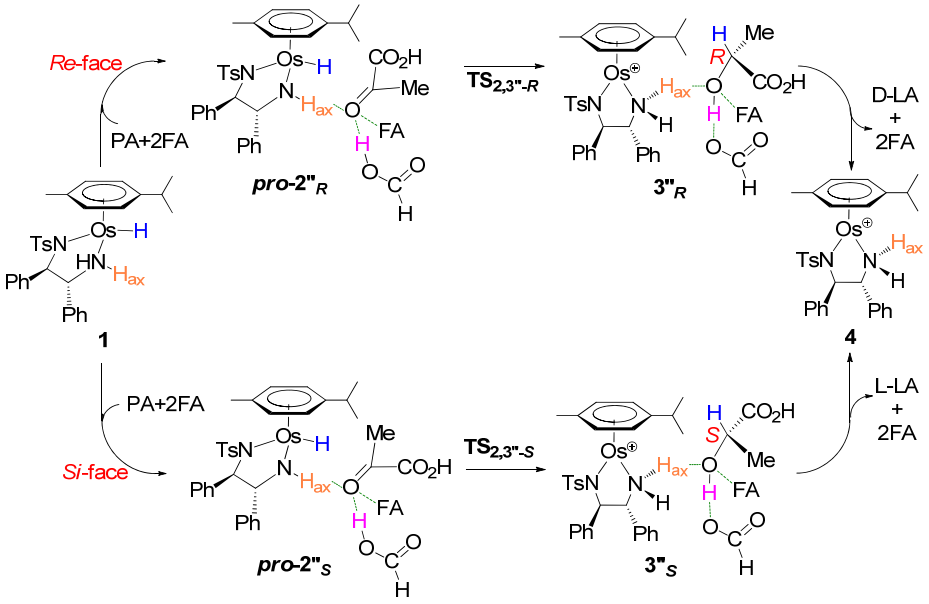

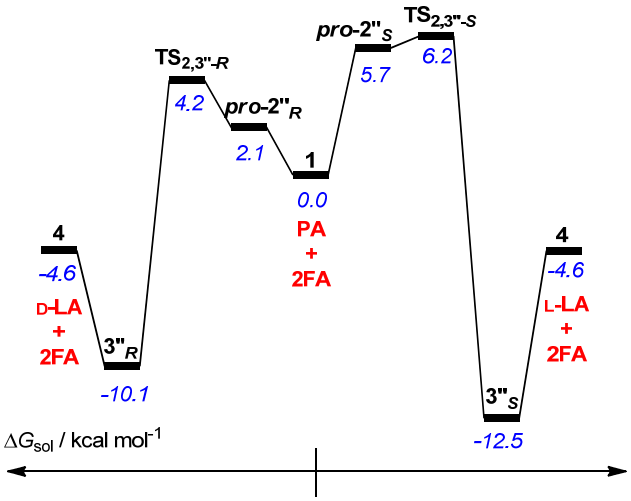

Figure S3. Free energy profile for the hydrogenation of PA catalysed by **1** with the presence of two FA molecule in calculations.

The mechanism for the hydrogenation of PA catalysed by **1** with the participation of two FA molecule is shown in Scheme S2. The corresponding free energy profile is shown in Figure S3. We found that the second FA molecule only has some weak hydrogen bond interactions with the reactant, but does not participate the proton transfer process. The calculated relative energies

are almost the same as the results with the participation of only one FA molecule. Therefore, although the reaction happens in the FA solvent, we believe one extra FA molecule in our computational reaction mechanism study is accurate enough because normal hydrogen bonds are usually 10 times stronger than nonspecific intermolecular interaction forces.[22]

6. The influence of water for hydride transfer

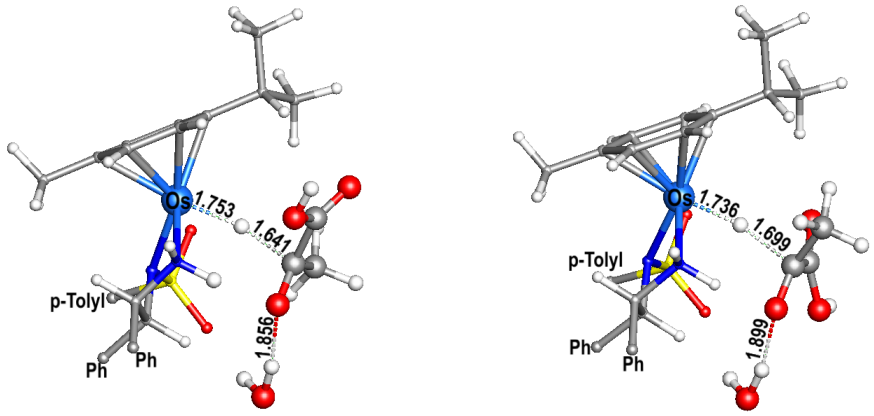

$\mathbf{TS_{2,3\text{-}R\text{-}H2O}}$ $\mathbf{TS_{2,3\text{-}S\text{-}H2O}}$

Figure S4. Optimized structures of $\mathbf{TS_{2,3\text{-}R\text{-}H2O}}$ (319*i* cm^{-1}) and its isomer $\mathbf{TS_{2,3\text{-}S\text{-}H2O}}$ (333*i* cm^{-1}). Bond lengths are in Å.

Table S4. Relative free energies of the enantio-determining state with the involvement of a formic acid or water molecule.

Additional molecule	ΔG_{sol} (**1** → $\mathbf{TS_{2,3\text{-}R}}$/$\mathbf{TS_{2,3\text{-}R\text{-}H2O}}$)	ΔG_{sol} (**1** → $\mathbf{TS_{2,3\text{-}S}}$/$\mathbf{TS_{2,3\text{-}S\text{-}H2O}}$)
	kcal mol^{-1}	
HCOOH	3.9	5.5
H_2O	5.5	7.7

In order to evaluate the possible influence of water to the reaction mechanism, we also calculated the enantio-determining hydride transfer process with the formic acid molecule replaced by a water molecule. Figure S4 shows the optimized transition state structures of $\mathbf{TS_{2,3\text{-}R\text{-}H2O}}$ or $\mathbf{TS_{2,3\text{-}S\text{-}H2O}}$. Different with the formic acid molecule, the H_2O molecule cannot provide a proton to carbonyl oxygen of pyruvic acid because of its weak acidity. The relative free energies of $\mathbf{TS_{2,3\text{-}R\text{-}H2O}}$ or $\mathbf{TS_{2,3\text{-}S\text{-}H2O}}$ are 5.5 or 7.7 kcal mol^{-1}, respectively, which are at least 1.6 kcal mol^{-1} higher than the corresponding relative free energies involving formic acid (Table S4). More importantly, formic acid is the hydrogen source in this catalytic transfer hydrogenation reaction.

7. Electrostatic potential map analysis

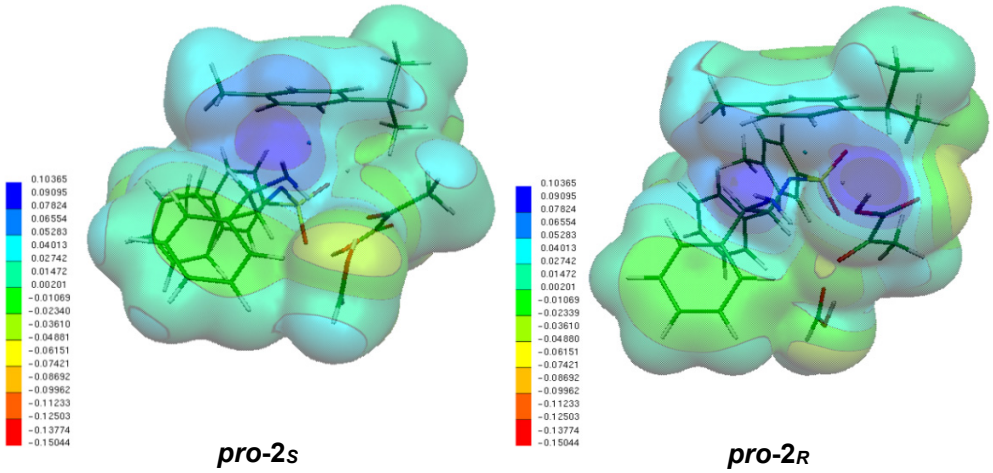

***pro*-2$_S$** ***pro*-2$_R$**

Figure S5. Electrostatic potential maps of ***pro*-2$_S$** and ***pro*-2$_R$** (isosurface value of 0.001 a.u.)

We also performed electrostatic potential analysis using Molekel 4.3.[23] As shown in Figure S5, the electrostatic potential distributions are in agreement with the conclusion that the η^6-*p*-cymene ligand and the carboxyl group in ***pro*-2$_R$** is in a more positive-enrichment region with primary electrostatic attractions.

References

1. M. J. Frisch, G. W. Trucks, H. B. Schlegel, G. E. Scuseria, M. A. Robb, J. R. Cheeseman, G. Scalmani, V. Barone, B. Mennucci, G. A. Petersson, H. Nakatsuji, M. Caricato, X. Li, H. P. Hratchian, A. F. Izmaylov, J. Bloino, G. Zheng, J. L. Sonnenberg, M. Hada, M. Ehara, K. Toyota, R. Fukuda, J. Hasegawa, M. Ishida, T. Nakajima, Y. Honda, O. Kitao, H. Nakai, T. Vreven, J. A. Montgomery, Jr., J. E. Peralta, F. Ogliaro, M. Bearpark, J. J. Heyd, E. Brothers, K. N. Kudin, V. N. Staroverov, T. Keith, R. Kobayashi, J. Normand, K. Raghavachari, A. Rendell, J. C. Burant, S. S. Iyengar, J. Tomasi, M. Cossi, N. Rega, J. M. Millam, M. Klene, J. E. Knox, J. B. Cross, V. Bakken, C. Adamo, J. Jaramillo, R. Gomperts, R. E. Stratmann, O. Yazyev, A. J. Austin, R. Cammi, C. Pomelli, J. W. Ochterski, M. L. Martin, K. Morokuma, V. G. Zakrzewski, G. A. Voth, P. Salvador, J. J. Dannenberg, S. Dapprich, A. D. Daniels, O. Farkas, J. B. Foresman, J. V. Ortiz, J. Cioslowski and D. J. Fox, *Gaussian 09*, *revision E.01*, Inc., Wallingford CT, 2013.
2. Y. Zhao and D. G. Truhlar, *Theor*. *Chem*. *Acc*., 2008, **120**, 215-241.
3. W. J. Hehre, R. Ditchfield and J. A. Pople, *J*. *Chem*. *Phys*., 1972, **56**, 2257-2261.
4. R. Krishnan, J. S. Binkley, R. Seeger and J. A. Pople, *J*. *Chem*. *Phys*., 1980, **72**, 650-654.
5. D. Figgen, K. A. Peterson, M. Dolg and H. Stoll, *J*. *Chem*. *Phys*., 2009, **130**, 164108.
6. J. Tomasi, B. Mennucci and R. Cammi, *Chem*. *Rev*., 2005, **105**, 2999-3094.
7. A. V. Marenich, C. J. Cramer and D. G. Truhlar, *J*. *Phys*. *Chem*. *B*, 2009, **113**, 6378-6396.
8. J. Manson, C. E. Webster and M. B. Hall, *Texas A&M University: College Station, TX*, *JIMP2*, *version 0.091*, 2006, a free program for visualizing and manipulating molecules.
9. F. M. Bickelhaupt and K. N. Houk, *Angew*. *Chem*. *Int*. *Ed*., 2017, **56**, 10070-10086.
10. W.-J. van Zeist and F. M. Bickelhaupt, *Org*. *Biomol*. *Chem*., 2010, **8**, 3118-3127.
11. O. N. Faza, C. S. López and I. Fernández, *J. Org*. *Chem*.; 2013, **78**, 5669-5676.
12. J. Tao, J. P. Perdew, V. N. Staroverov and G. E. Scuseria, *Phys*. *Rev*. *Lett*., 2003**, 91**, 146401.
13. C. Lee, W. Yang and R. G. Parr, *Phys*. *Rev*. *B,* 1988**, 37**, 785-789.
14. A. D. Becke, *J*. *Chem*. *Phys*., 1993**, 98**, 5648-5652.
15. J. P. Perdew, J. A. Chevary, S. H. Vosko, K. A. Jackson, M. R. Pederson, D. J. Singh and C. Fiolhais, *Phys*. *Rev*. *B,* 1992**, 46**, 6671-6687.
16. J. P. Perdew, J. A. Chevary, S. H. Vosko, K. A. Jackson, M. R. Pederson, D. J. Singh and C. Fiolhais, *Phys*. *Rev*. *B,* 1993**, 48**, 4978-4978.
17. S. Grimme, J. Antony, S. Ehrlich and H. Krieg, *J*. *Chem*. *Phys*., 2010, **132**, 154104.
18. J.-D. Chai and M. Head-Gordon, *J*. *Chem*. *Phys*., 2008, **128**, 084106.
19. J.-D. Chai and M. Head-Gordon, *Phys. Chem. Chem. Phys.,* 2008**, 10**, 6615-6620.
20. M. Ernzerhof and J. P. Perdew, *J. Chem*. *Phys*., 1998**, 109**, 3313-3320.
21. D. Andrae, U. Haeussermann, M. Dolg, H. Stoll and H. Preuss, *Theor. Chim. Acta*, 1990, **77**, 123-141.
22. C. Reichardt and T. Welton, *Solvents and Solvent Effects in Organic Chemistry*; 4th ed.; Wiley-VCH, 2010.
23. P. Flükiger, H. Lüthi, S. Portmann and J. Weber, *Molekel 4.3*, Swiss Center for Scientific Computing, Manno, Switzerland, 2000, p. 2002.